Miner Petrol (2016) 110:681–692
DOI 10.1007/s00710-016-0439-1

ORIGINAL PAPER

Mineralogy and origin of coarse-grained segregations in the pyrometallurgical Zn-Pb slags from Katowice-Wełnowiec (Poland)

R. Warchulski[1] · A. Gawęda[1] · J. Janeczek[1] · M. Kądziołka-Gaweł[2]

Received: 20 December 2015 / Accepted: 9 March 2016 / Published online: 21 March 2016

Abstract The unique among pyrometallurgical slags, coarse-grained (up to 2.5 cm) segregations (up to 40 cm long) rimmed by "aplitic" border zones occur within holocrystalline historical Zn-smelting slag in Katowice, S Poland. Slag surrounding the segregations consists of olivine, spinel series, melilite, clinopyroxene, leucite, nepheline and sulphides. Ca-olivines, kalsilite and mica compositionally similar to oxykinoshitalite occur in border zones in addition to olivine, spinel series and melilite. Miarolitic and massive pegmatite-like segregations are built of subhedral crystals of melilite, leucite, spinel series, clinopyroxene and hematite. Melilite, clinopyroxenes and spinels in the segregations are enriched in Zn relatively to original slag and to fine-grained border zones. The segregations originated as a result of crystallization from residual melt rich in volatiles (presumably CO_2). The volatile-rich melt was separated during fractional crystallization of molten slag under the cover of the overlying hot (ca. 1250 °C) vesicular slag, preventing the escape of volatiles. That unique slag system is analogous to natural magmatic systems.

Editorial handling: J. Elsen

✉ R. Warchulski
rwarchulski@us.edu.pl

[1] Faculty of Earth Sciences, University of Silesia, Będzińska 60, 41-200 Sosnowiec, Poland

[2] Faculty of Mathematics, Physics and Chemistry, University of Silesia, Bankowa 14, 40-007 Katowice, Poland

Introduction

Pyrometallurgical slags from base-metal smelting have recently been studied extensively mainly with the purpose of assessing their environmental impact for many of them contain elevated concentrations of potentially toxic metals, including As, Cd, Cu, Pb and Zn (e.g. Ettler et al. 2001; Puziewicz et al. 2007; Álvarez-Valero et al. 2009, Piatak and Seal 2010; Vítková et al. 2010; Kierczak et al. 2010; Ettler and Johan 2014). Those metals may be partitioned among phases with different leaching potential during weathering. Therefore, the detailed knowledge of phase composition of slags is prerequisite for understanding their leaching behaviour. Pyrometallurgical slags are also interesting from the petrological perspective, as their structures, textures and phase composition are analogous to those in mafic volcanic rocks (e.g. Vernon 2004; Puziewicz et al. 2007).

The chemical and mineral composition of slags depend on the composition of primary ore, additives used in the smelting processes (e.g. fluxing material) and on the smelting technology. Slags originated from Zn and Pb smelting are composed mainly of silicates (melilite series, clinopyroxenes, olivine, Ca-olivines, and Ca-plagioclases) and spinel series. Numerous other phases may also be present either as dominant or minor constituents depending on local conditions of their formation.

The grain size of crystalline phases in slags depends on the thermal history of a slag bed but most crystalline slags are fine to medium-grained with skeletal/dendritic crystals. In this paper we report the occurrence of coarse-grained segregations in holocrystalline slags deposited at a site of a historic, zinc smelter in Katowice, the capital of the Upper Silesia region in southern Poland. The main goal of this paper is to decipher

the origin of the segregations and to determine the crystallization sequence in different zones of the segregations, the partition of elements to different crystalline phases in different slag zones and finally to construct the model of formation for the unusual pegmatite-like segregations. It is a common practise to use mineral names for designating analogous crystalline phases that compose slags. We will follow that convention throughout the article.

Site description

Samples were collected from remnants of a slag bed at a site of historic zinc and lead smelting plant located in Wełnowiec, a district of Katowice (Fig. 1a). The zinc smelter was built in 1873 in place of a former iron smelter. The smelting plant in Katowice-Wełnowiec was among the largest single zinc producers in Europe. The smelting plant used the method invented at the end of the eighteenth century by Johann Christians Ruberg and is called the Silesian process (Greiner 2004). The ore concentrate was loaded to 288 muffles (retorts) horizontally inserted into the continuously heated furnaces. Zinc vaporized at 1200–1300 °C and condensed upon cooling in a clay tube (condenser) attached to each muffle. Finally, metal blocks weighing 20 kg each were formed from liquid zinc. The horizontal muffles allowed a constant loading of batch and fuel (coke) without cooling the system. The last furnace of that type was decommissioned in the Katowice-Wełnowiec plant in 1980. Initially, the smithsonite ore (calamine) was smelted; however, it was soon substituted by the Zn and Pb-sulphide ore mined in the Upper Silesian Mississippi Valley-type deposits hosted by the mid-Triassic dolomites. The ore consists of collomorphic sphalerite (zinc blende), galena, pyrite, marcasite, and locally wurtzite and brunckite (e.g. Heijlen et al. 2003). Dolomite, barite, and calcite are gangue minerals. Of environmental concern is the fact, that the light-coloured collomorphic aggregates of sphalerite are enriched in Cd up to 1.5 wt.%; whereas, As and Tl tend to concentrate in galena (up to 4.9 wt.% As and 0.08 wt.% Tl) and in marcasite/pyrite (up to 1.6 wt.% As and 0.09 wt.% Tl) (Mayer and Sass-Gustkiewicz 1998). The question how these elements migrate to slag phases is still open and would be investigated in the subsequent paper.

Slags from Katowice-Wełnowiec have been used for road constructions and only remnants of the bottom portion of the slag-pile that covered an area of 24 ha are preserved as an industrial heritage (Fig. 1). The exact age of the investigated slag is unknown. Most probably it was deposited at the beginning of the twentieth century, when the Silesian method of zinc smelting was a common practise.

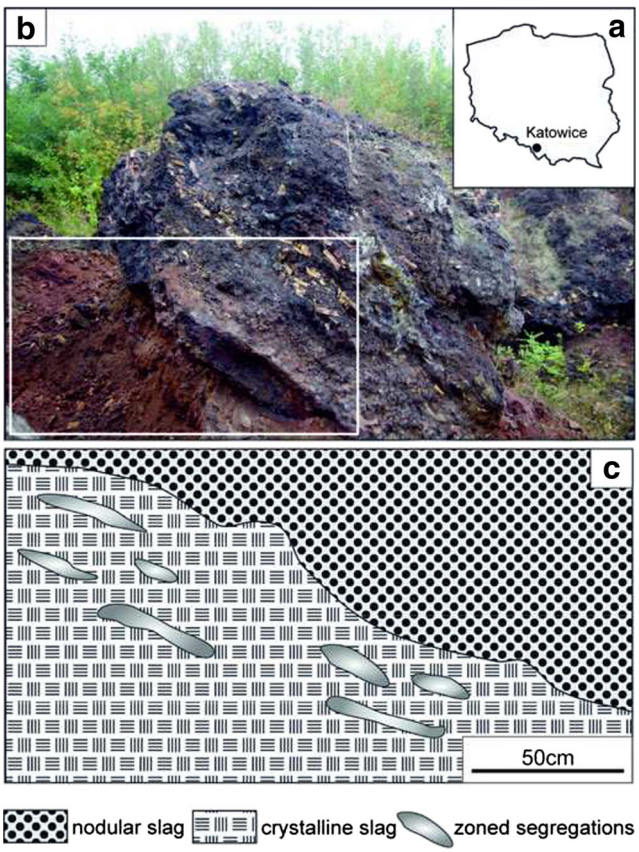

Fig. 1 Remnants of the slag pile in the Katowice-Wełnowiec slag-dump. Inset shows the location of Katowice in Poland (**a**). The framed area in (**b**) is explained in the generalized schematic illustration (**c**)

Experimental

Thirty samples were collected at the Katowice-Wełnowiec site. Samples were selected on the basis of macroscopic observations to represent all distinguishable slag types. Before further preparations samples were cleared from the soil and dried in 22 °C for seven days. Thin sections of slags were examined using an Olympus BX-51 polarizing microscope and an analytical scanning electron microscope (SEM; FET Philips XL30) equipped with an energy-dispersive spectrometer. Electron probe micro-analyses (EPMA) and backscattered electron (BSE) imaging of phases were performed using electron probe micro-analyser CAMECA SX 100 (Inter-Institutional Laboratory of Microanalysis of Minerals and Synthetic Materials, the Warsaw University). Analyses were performed at 15 keV accelerating voltage, 10–20.1 nA beam current, and beam diameter of up to 5 μm. Standards included: Ag – Ag_2Te; Al – $KAlSi_3O_8$; As – GaAs; Ba – $BaSO_4$; Bi – Bi_2Te_3; Ca – $CaSiO_3$; Cd – CdS; Ce – CeP_5O_{14}; Cl – $Na_4AlBeSi_4O_{12}Cl$; Co – CoO; Cr – Cr_2O_3; Cu – $CuFeS_2$; F – $Ca_5(PO_4)_3(F,Cl,OH)$; Fe – Fe_2O_3; K – $KAlSi_3O_8$; La – LaB_6; Mg – $MgCaSi_2O_6$; Mn – $MnCO_3$;

Na – $NaAlSi_3O_8$; Nb – Nb; Nd – $NdGaO_3$; Ni – NiO; P – $Ca_5(PO_4)_3(F, Cl, OH)$; Pb – PbS, $PbCrO_4$; Pr – Pr synthetic glass; S – $BaSO_4$, $CuFeS_2$, ZnS; Sb – Sb_2Te_3, InSb; Se – Bi_2Se_3; Si – $CaSiO_3$; Sr – $SrTiO_3$; Ti – TiO_2; V – V_2O_5; Y – YP_5O_{14}; Zn - ZnS.

X-ray powder diffraction patterns were obtained using a diffractometer PANalytical X'PERT PRO – PW 3040/60 (X'PERT HighScore Plus software) and Co $K_{\alpha 1}$ radiation (Fe filter). Operating conditions were 45 kV and 30 mA. The X'PERT HighScore Plus software was applied for data processing. The elimination algorithm of Ladell et al. (1975) was used for Kα2 stripping.

Mössbauer spectra of bulk samples were recorded at room temperature using a constant acceleration spectrometer with a ^{57}Co:Pd source. A metallic α-Fe powder absorber was used for velocity and isomer shift calibrations. The Sterns et al. (1998) methodology was used for the interpretation of the obtained Mössbauer spectra.

Results

Generalities

The investigated slag is holocrystalline, fine- to medium-grained (0.2–1.0 mm) and is composed of olivine, pyroxene, spinel series, melilite series and subordinate leucite, nepheline and sulphides (Warchulski and Szopa 2014). The holocrystalline slag is overlain by fine-grained vesicular slag mixed with debris of building materials (Fig. 1b). Numerous elongate, coarse-grained segregations occur in the uppermost layer of the holocrystalline slag aligned parallel to the contact with the overlying vesicular slag (Fig. 1c). The segregations are ellipsoidal or flattened irregular with large aspect ratio (3:1 to 5:1) and they range in size from 10 to 40 cm along their major axis (Fig. 2). There are two types of segregations: (a) with crystal lined cavities, referred hereafter as miarolitic segregations (Fig. 2a, b), and (b) massive segregations with subhedral crystals (Fig. 2c). Melilite, spinel, and pyroxene are major phases in both types of segregations. Subordinate hematite is confined to the miarolitic segregations; whereas, leucite has been observed in the massive segregations. There is a fine-grained (0.4–0.6 mm) equigranular border zone between slag and the segregations composed of olivine, spinel, melilite, pyroxenes, monticellite-kirschsteinite, and sulphides. The transition from the border zone to the segregations is marked by a sharp increase in crystal size of up to 25 mm across. Walls of cavities in the miarolitic segregations are lined with euhedral crystals of melilite overgrown by pyroxene, leucite, spinel and hematite (Fig. 3a-c). Locally, apatite has been observed. While phase assemblages of both types of segregations and their corresponding border zones are almost identical they differ in mineral chemistry.

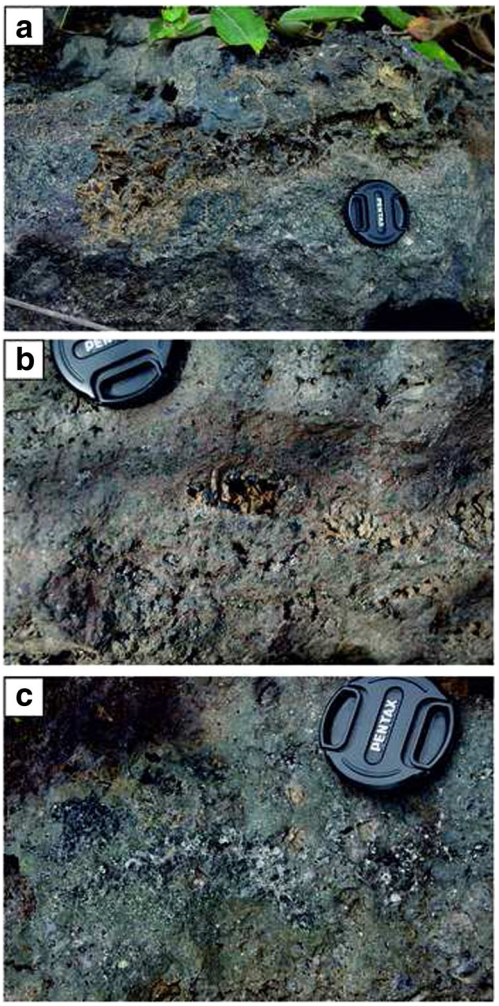

Fig. 2 Miarolitic segregations (**a, b**) and massive segregation with leucite-rich core (**c**) in slag

Mineral chemistry

Oxides

Spinel-group phases occur in the holocrystalline slag and in the segregations as euhedral, zoned crystals up to 400 μm across (Fig. 4a, b). They are composed of a multicomponent solid solution of franklinite ($ZnFe_2O_4$) - gahnite ($ZnAl_2O_4$) - magnetite ($FeFe_2O_4$) - hercynite ($FeAl_2O_4$) (Table 1; Fig.5a) enriched in Mg, Mn and Ti. There are significant differences in chemical compositions between spinel phases in the segregations, their border zones and the surrounding slag (Table 1). Spinels from the regular slag are represented by Mg-spinel with magnetite compound (Fig. 5), and are enriched in Ti relative to spinels from the segregations (Table 1). Spinels in the border zone of segregation span a wide range of compositions from Mg- and Al-rich to enriched in magnetite component (Fig. 5). Spinels in the border zones of miarolitic segregations and in the massive segregations show different

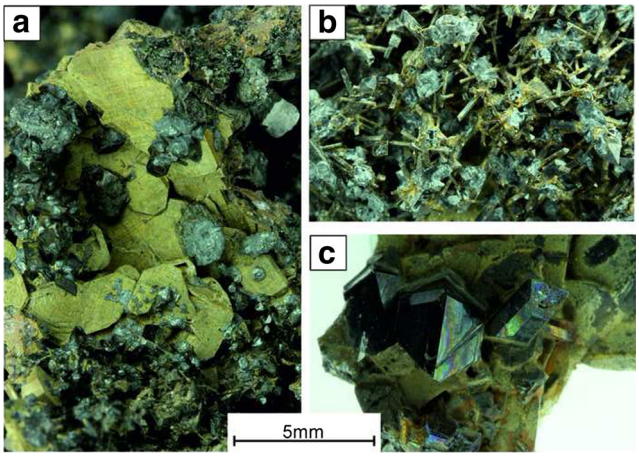

Fig. 3 Mineral phases in miarolitic cavity: (**a**) platy crystals of melilite overgrown by clinopyroxene with different morphology (**b, c**)

compositional trends (Fig. 5). While there are increasing concentrations of magnetite components in both groups of spinels, from around 10 mol% to over 80 mol% with a gap between 40 and 60 mol%, spinels from the border zone of the miarolitic segregations are relatively enriched in Mg and poorer in Zn. Trends in the border zones corresponds to spinel zoning distinguished in this slag parts: the Mg-Al core and the rim enriched in Fe. Spinels in both types of segregations are Zn-rich and can be grouped into the franklinite-dominated and gahnite-dominated compositions (Fig. 5a).

Mössbauer spectroscopic measurements were applied to distinguish different oxidation states of iron. Mössbauer spectra of spinel-pyroxene aggregates from the segregations show the overlapping magnetic and paramagnetic components (Fig. 6). The relatively small amount of Fe^{3+} in the magnetic component (Table 2) probably results from the extensive substitution of Fe^{3+} by Al^{3+}. This is confirmed by the Al distribution in zoned crystals (Fig. 4a). The chemical composition of the core (M1) is approximated by the formula $(Mg, Zn)Al_2O_4$, whereas rims (M2) are Al-depleted and their chemical compositions can be expressed as $(Fe^{2+},Mn^{2+})(Fe^{3+},Ti, Mn^{4+})_2O_4$. The occurrence of hematite as the latest phase in the segregations suggests oxidative conditions. Some of Fe^{+3} in hematite is substituted by Al, Ti, Mg, Mn and Zn (Table 1).

Silicates and aluminosilicates

Melilite is common phase in the holocrystalline slag and it is a predominant phase in the segregations. Its yellowish, platy or locally dendritic crystals up to 25 mm across, show perfect cleavage (Figs. 3a). They are overgrown by pyroxene and oxide minerals (Figs. 3a, c and 4d). The mean composition of the melilite series corresponds to the alumo-akermanite - hardystonite solid solution: $(Ca_{1.93}Na_{0.07}K_{0.02})(Mg_{0.51}Fe_{0.19}Zn_{0.19}Al_{0.10}Mn_{0.01})(Si_{1.96}Al_{0.04})O_7$ (Table 1; Fig. 7). Melilite crystals from the massive segregations have the highest concentrations of Zn and represent the $Ca_2MgSi_2O_7$ - $Ca_2ZnSi_2O_7$ solid solution with less than 10 % of the $Ca_2FeSi_2O_7$ endmember (Fig. 7). Melilite from the miarolitic segregations is relatively depleted in Zn and shows variable

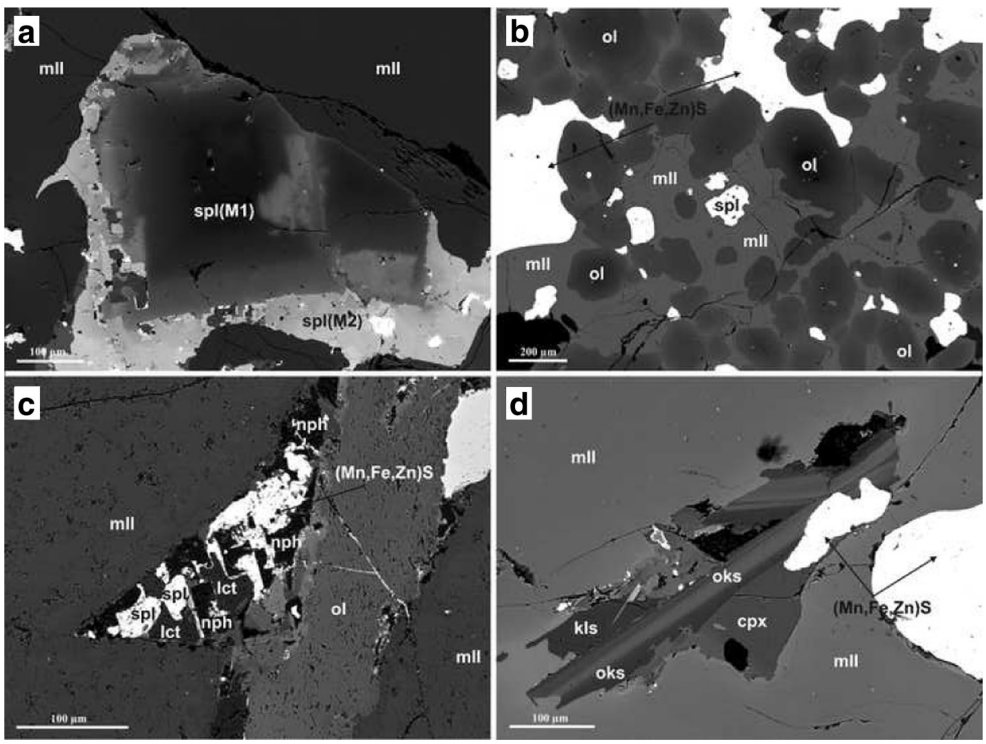

Fig. 4 BSE images of: (**a**) zoned magnetite within melilite; (**b**) rounded crystals of zoned olivine surrounded by mellite and blebs of (Mn,Fe,Zn)S; (**c**) nepheline, spinel, leucite and (Mn,Fe,Zn)S in the interstices between melilite and olivine in slag; (**d**) oxykinoshitalite-like mica, clinopyroxene and kalsilite within melilite. Abbreviations: cpx – clinopyroxene; kls – kalsilite; lct – leucite; mll – melilite; nph – nepheline; oks – oxykinoshitalite; ol – olivine; spl – spinel; spl(M1–2) – refer to spinel compositions (see text)

Table 1 EPMA data (wt.%) for spinel, hematite, melilite and clinopyroxene from slag, border zones and segregations

	spl I	spl II	spl III	hem	mll I	mll II	mll III	cpx I	cpx II	cpx III
SiO_2	–	–	–	–	41.95	40.72	42.01	49.22	46.11	45.54
TiO_2	2.18	0.33	0.13	1.19	0.06	0.05	0.12	0.46	0.21	0.26
Al_2O_3	14.93	49.36	3.68	2.49	3.92	1.68	2.16	0.90	7.22	7.95
Fe_2O_{3calc}	49.49	18.00	67.01	95.16	–	–	–	6.10	9.90	6.05
FeO_{calc}	25.06	11.25	2.70	0.63	5.21	6.24	0.75	11.04	0.10	5.53
ZnO	2.12	5.77	18.43	0.32	1.84	5.37	8.49	0.14	0.58	0.61
MnO	1.99	0.46	2.40	0.21	0.46	0.47	0.24	3.09	0.60	0.47
MgO	4.18	14.6	4.78	0.22	7.44	6.29	7.93	6.12	10.14	9.81
CaO	–	–	–	–	36.66	38.28	37.66	20.10	24.57	23.84
Na_2O	–	0.21	0.46	–	1.82	0.13	0.70	1.80	1.05	0.04
K_2O	–	–	–	–	0.09	0.43	0.54	–	–	–
Total	99.95	99.98	99.59	100.22	99.43	99.66	100.58	98.96	100.46	100.09
a.p.f.u. (atoms per formula units)										
Si	–	–	–	–	1.97	1.96	1.98	1.95	1.73	1.73
Ti^{4+}	0.06	0.01	0.00	0.02	0.00	0.00	0.01	0.01	0.01	0.01
Al	0.61	1.61	0.16	0.08	0.21	0.10	0.12	0.04	0.32	0.36
$Fe^{3+}{}_{calc}$	1.29	0.38	1.88	1.87	–	–	–	0.18	0.28	0.17
$Fe^{2+}{}_{calc}$	0.72	0.26	0.08	0.01	0.20	0.25	0.03	0.37	0.00	0.18
Zn	0.05	0.12	0.51	0.01	0.06	0.20	0.29	0.00	0.02	0.02
Mn	0.05	0.01	0.07	0.00	0.02	0.02	0.01	0.10	0.02	0.01
Mg	0.22	0.60	0.27	0.01	0.52	0.45	0.56	0.36	0.57	0.56
Ca	–	–	–	–	1.84	1.98	1.9	0.85	0.99	0.97
Na	–	0.01	0.03	–	0.17	0.01	0.07	0.14	0.08	0.00
K	–	–	–	–	0.01	0.03	0.03	–	–	–
O^{2-}	4.00	4.00	4.00	3.00	7.00	7.00	7.00	6.00	6.00	6.00

spl–spinel, hem–hematite, mll–melilite, cpx–clinopyroxene, I–slag, II–border zones, III-segregations

concentrations of Fe and Mg (Fig. 7). Melilite from the border zone of the massive segregations has intermediate concentrations of Zn between Zn-rich melilite from the massive segregations and Zn-poor melilite from miarolitic segregations. Melilite from the border zone of the miarolitic segregations is Mg-rich (>70 % $Ca_2MgSi_2O_7$) and Zn-poor. All

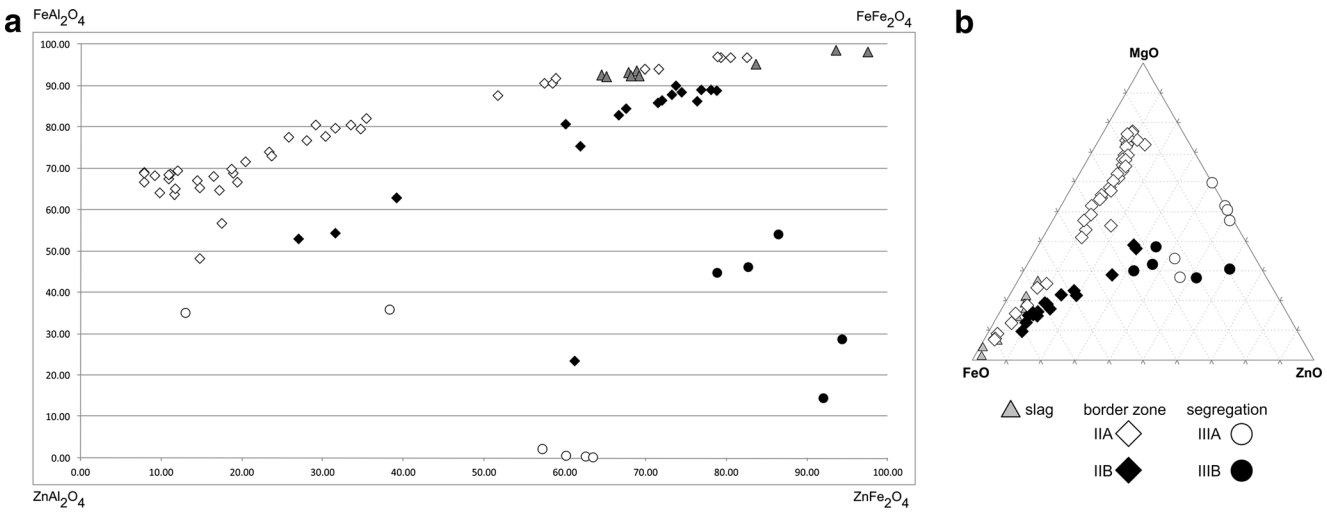

Fig. 5 (**a**) The gahnite $ZnAl_2O_4$ - hercynite $FeAl_2O_4$ - franklinite $ZnFe_2O_4$ - magnetite $FeFe_2O_4$ quadrilateral diagram showing compositions of spinel series in crystalline slag, border zones and segregations. (**b**) Compositional variations of spinel series in the ternary diagram MgO-FeO-ZnO. Abbreviations: IIa – border zone of miarolitic segregations; IIb – border zone of massive segregations; IIIa – miarolitic segregation; IIIb – massive segregations

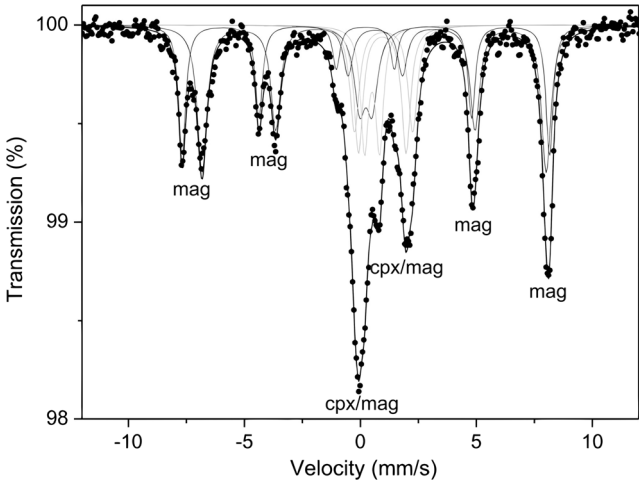

Fig. 6 Mössbauer spectrum of the magnetite-pyroxene aggregate from miarolitic segregation. Solid dots – experimental data; solid lines – fitted curves; cpx- clinopyroxene, mag – magnetite

melilite crystals are compositionally homogeneous (Fig. 4). Unit cell parameters of melilite from the miarolitic segregations calculated for the space group $P\bar{4}2_1m$ are a_0 = 7.84 Å, c_0 = 5.01 Å. They are similar to unit cell parameters of akermanite and hardystonite in accordance with EPMA data.

Pyroxene chemical compositions (Table 1) are dominated by a diopside – hedenbergite solid solution with elevated concentrations of the wollastonite compound (Fig. 8a). Ca-rich pyroxene locally occurs in the massive segregations (Fig. 8a). The chemical composition of pyroxenes is further complicated by the substitution of Mg and Fe by Al, Zn, Na, Mn, and Ti (Table 1). Zinc concentration in pyroxenes increases from Fe- and Mg-dominated compositions in the slag, through border zone of the segregations to Zn-rich internal part of the segregations (Fig. 8b). Approximately 30 % of Fe in pyroxenes from the segregations is trivalent as suggested by the Mössbauer spectra of pyroxene-spinel aggregates (Fig. 6). Unit cell parameters of idiomorphic, prismatic pyroxene crystals from the miarolitic segregation calculated for the space group C2/c are: a_0 = 9.76 Å; b_0 = 8.92 Å, c_0 = 5.28 Å; β = 106°. Pyroxene crystals are zoned with the core enriched in Na, Mn, Fe^{2+}, Mg, and Si; whereas, rim has elevated concentrations of Fe^{3+}, Al, and Ti.

Table 2 Hyperfine interaction parameters, obtained from Mössbauer spectra

	Is (mm/s)	Qs (mm/s)	H (T)	A (%)
Pyroxene	0.558 ± 0.018	0.646 ± 0.019	-	10.7
	1.056 ± 0.013	2.504 ± 0.048	-	11.4
	1.000 ± 0.024	2.052 ± 0.050	-	12.9
Magnetite	0.290 ± 0.0061	0.536 ± 0.096	-	9.8
	0.672 ± 0.006	0.025 ± 0.006	46.27 ± 0.01	33.3
	0.277 ± 0.005	−0.011 ± 0.005	49.28 ± 0.04	21.9

Is–isomer shift, Qs–quadrupole splitting, H–hyperfine splitting, A–contribution

Olivine occurs in the slag and in the border zones. Olivine in the slag is fayalite-rich (Fa/Fo = 0.76) and is enriched in Mn relative to olivine in the border zone, in which forsteritic olivine prevails (Fa/Fo = 0.34) (Table 3). Olivine in the border zone is slightly enriched in Zn (2.76 wt.%) compared to olivine from the slag (1.0 wt.% ZnO). Calcium content in all examined olivines is similar, ranging from 3.3 mol% in the slag to 3.8 mol% in the border zone (Table 3). Some olivine crystals are zoned (Fig. 4b) with the core enriched in Fe, Mn, and Ca relative to the Mg-rich rim.

Kirschsteinite – monticellite solid solution was distinguished in the border zone only. Crystals of this phase has simple composition with minor substitutions of Mn, Na and Zn for Mg and Fe (Table 3).

Kalsilite and nepheline are rare in the slag (Fig. 4c and d). Both have a simple chemical composition that does not deviate significantly from the ideal composition (Table 3).

White leucite crystals occur in interstices between other phases in the slag and in the border zone of the segregations (Figs. 2c). Leucite chemical composition is complex with the noticeable presence of Ce (Table 3).

Mica crystals up to 400 μm across occur in the border zone of the segregations (Fig. 4d). The average chemical composition of the mica corresponds to oxykinoshitalite and can be expressed as: $(K_{0.86}Ba_{0.15})(Fe^{2+}_{0.39}Mn_{0.02}ZnO_{0.04}Mg_{2.49}Na_{0.06})(Si_{2.82}Al_{1.20})O_{10}(O,OH)_2$. The elements Ca and Sb were detected in some EPM analyses of mica (Table 4). The examined mica is zoned with Ba and Al concentrated in the core, and K, Si and Fe in the rim (Fig. 4d; Table 4).

Phosphates

Acicular crystals of a phase compositionally close to fluorapatite ($Ca_{5.15}[PO_4]_{3.00}F_{0.76}$) with some LREE and Y (Table 4) occur as inclusions in late pyroxene crystals from the miarolitic segregations (Fig. 9).

Sulphides

Sulphides representing MnS-ZnS-FeS solid solution are dispersed within a groundmass of slag and the border zone. The Mn content is up to 4.53 wt.% (Table 5). They significantly differ from sulphides in the host ore-bearing rocks, which are almost pure ZnS, with subordinate Fe substitutions (Rajchel 2008).

Pyrrhotite has been observed in slag surrounding the segregations and rarely in the border zones. Pyrrhotite has rather uniform chemical composition with minor substitutions of Mn, Cu, Co and Ni for Fe (Table 5). Chalcopyrite occurs as a subordinate phase only in slag surrounding the segregations. Small amounts of Ag, Zn, Mn, Co, Ni have been detected in chalcopyrite (Table 5). Only one crystal of galena has been

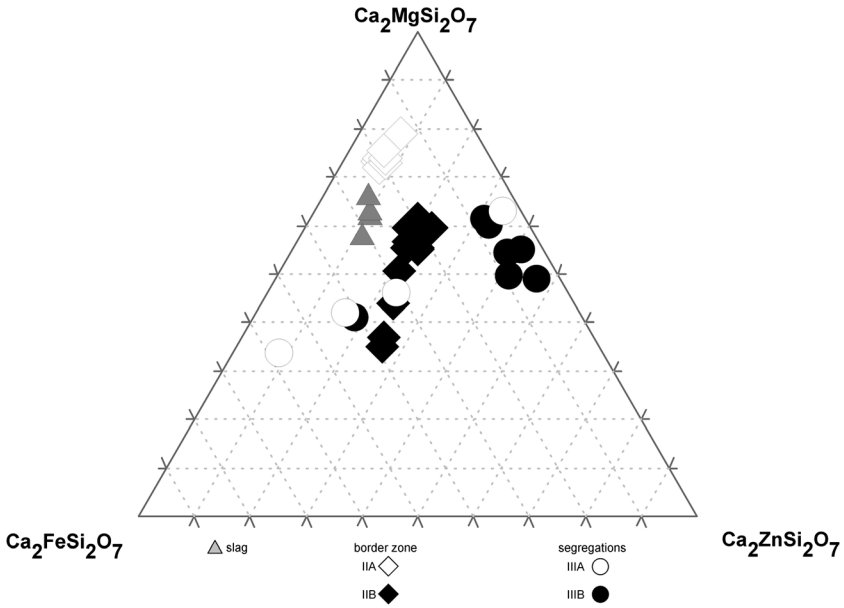

Fig. 7 The melilite ternary diagram $Ca_2MgSi_2O_7$ – $Ca_2FeSi_2O_7$ – $Ca_2ZnSi_2O_7$ showing compositions of melilite in slag, border zone and segregations. Abbreviations: IIa – border zone of miarolitic segregations; IIb – border zone of massive segregations; IIIa – miarolitic segregation; IIIb – massive segregations

found in the analysed slags. Its chemical composition is complex with numerous substitutions for Pb (Table 5).

Discussion

The sequence of crystallization

Calcium-rich silicates: melilite, clinopyroxenes, and Ca-olivines are predominant phases in the slags and in the segregations. The enrichment in Ca most probably resulted from the Ca-bearing fluxing material added to the charge and, consequently partitioning of Ca into the silicate melt during metallurgical process. Iron sulphides (pyrite and marcasite) associated with the Zn-Pb ore were the source of Fe in spinels, olivines and clinopyroxenes (Warchulski et al. 2015).

Based on spatial relations between mineral phases the following paragenetic sequence has been established in the slag: olivine and spinel → melilite → clinopyroxene (Fig. 10). Leucite, nepheline and sulphides crystallized from residual melt as the latest phases. Similar sequence of crystallization commonly occurs in pyrometallurgical slags regardless of Zn smelting technology (e.g. Ettler et al. 2001; Puziewicz et al. 2007; Warchulski et al. 2015).

The sequence of crystallization in the border zone of segregations is similar to the slag. Crystallization began with olivine followed by spinel and melilite. The interstices between those phases were filled by monticellite – kirschteinite solid solution, second generation of spinel and sulphides. Locally, mica (similar to oxykinoshitalite), pyroxene and kalsillite crystallized between melilite crystals. Oxykinoshitalite was described as a new species from olivine nephelinite composed of olivine, clinopyroxene,

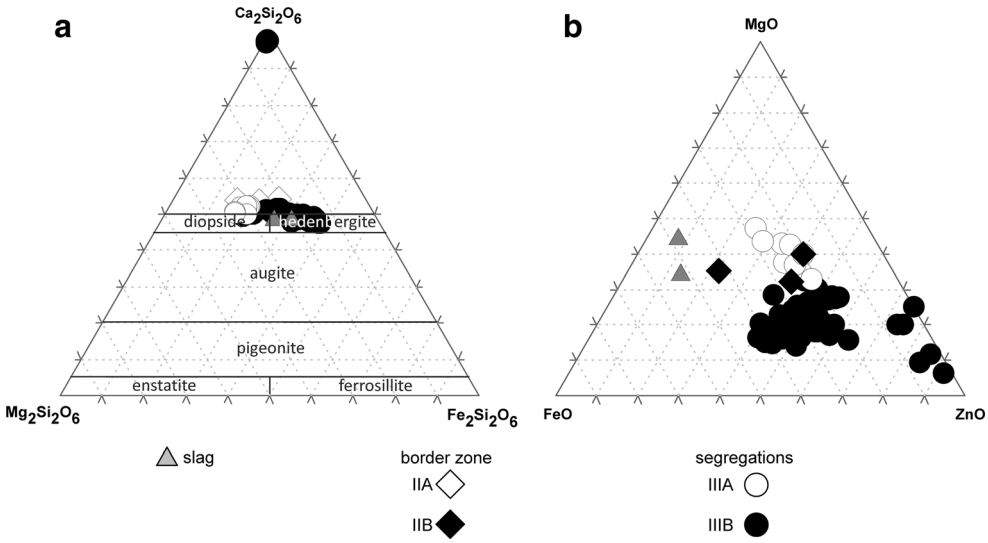

Fig. 8 (**a**) The pyroxene ternary diagram showing compositions of pyroxenes from slag, border zones and segregations. (**b**) Pyroxene compositions plotted in the ternary diagram MgO-FeO-ZnO. Abbreviations: IIa – border zone of miarolitic segregations; IIb – border zone of massive segregations; IIIa – miarolitic segregation; IIIb – massive segregations

Table 3 EPMA data (wt.%) for olivine, monticellite – kirschsteinite solid solution, kalsilite, nepheline and leucite from slag, border zones and segregations

	ol I	ol II	mtc-kir	kls	nph	lct I	lct II	lct III
Sb_2O_5	–	–	–	0.70	–	–	–	–
SiO_2	34.7	37.61	36.63	39.95	42.51	53.76	54.78	54.68
Al_2O_3	–	–	–	30.81	27.15	23.76	23.23	23.77
Ce_2O_3	–	–	–	–	–	0.46	0.01	0.21
Fe_2O_{3calc}	–	–	–	–	–	0.50	1.45	0.89
FeO_{calc}	32.94	21.19	10.19	0.50	9.66	–	–	–
ZnO	1.00	2.76	0.79	–	0.12	–	–	–
MnO	4.92	1.46	0.65	–	0.33	–	–	–
MgO	23.88	34.61	20.72	0.12	1.03	–	–	–
CaO	2.37	2.86	30.88	–	0.75	–	–	–
BaO	–	–	–	–	0.21	1.30	0.29	0.92
Na_2O	–	–	–	0.12	13.48	–	–	–
K_2O	–	–	–	28.62	5.69	20.74	20.91	20.81
Total	99.81	100.49	99.86	100.82	100.93	100.52	100.67	101.28
a.p.f.u. (atoms per formula units)								
Sb^{5+}	–	–	–	0.01	–	–	–	–
Si	0.99	1.00	1.00	1.04	1.06	1.97	1.99	1.99
Al	–	–	–	0.94	0.80	1.02	0.99	1.02
Ce^{3+}	–	–	–	–	–	0.01	0.00	0.00
$Fe^{3+}{}_{calc}$	–	–	–	–	–	0.01	0.04	0.02
$Fe^{2+}{}_{calc}$	0.79	0.47	0.23	0.01	0.20	–	–	–
Zn	0.02	0.05	0.02	–	0.00	–	–	–
Mn	0.11	0.03	0.01	–	0.01	–	–	–
Mg	1.02	1.37	0.84	0.00	0.04	–	–	–
Ca	0.07	0.08	0.9	–	0.02	–	–	–
Ba	–	–	–	–	0.00	0.02	0.00	0.01
Na	–	–	–	0.01	0.65	–	–	–
K	–	–	–	0.95	0.18	0.97	0.98	0.96
O^{2-}	4.00	4.00	4.00	4.00	4.00	4.00	4.00	4.00

ol-olivine, mtc-kir-monticellite–kirschsteinite solid solution, kls–kalsilite, nph–nepheline, lct–leucite, I–slag, II–border zones, III-segregations

Fe–Ti oxide, nepheline, calcite, apatite and K-rich feldspar (Kogarko et al. 2005), an assemblage analogous to the examined slag. The occurrence of oxykinoshitalite in the border zone suggests local enrichment in water, which is a rather uncommon feature in pyrometallurgical slags. This may be caused by interaction with rainwater after and/or during slag deposition.

The crystallization conditions of the monticellite – kirschteinite solid solution in the border zone can be inferred from the univariant pressure-temperature curves determined by Walter (1963) and experimentally confirmed by Gustafson (1974) and defined by the following reactions:

$$2Ca_2MgSi_2O_7 + Mg_2SiO_4 \Leftrightarrow 3CaMgSiO_4 + CaMgSi_2O_6 \quad (1)$$

$$6CaSiO_3 + 2Fe_3O_4 \Leftrightarrow 6CaFeSiO_4 + O_2 \quad (2)$$

Those reactions occur between ~900 and 1400 °C at atmospheric pressure (Kushiro and Yoder 1964) and were already noted in other slags from Upper Silesia (Warchulski et al. 2015; Puziewicz et al. 2007).

The sequence of crystallization in the massive segregations differs from the miarolitic segregations by the lack of hematite. Spinel compositionally close to franklinite was the first phase to crystallize in the massive segregations possibly due to the increased oxygen fugacity during the reaction [2] in the border zone. Melilite crystallized next and was followed by pyroxene and leucite. Crystallization in the miarolitic segregations began with centimetre-sized euhedral melilite followed by often intergrown Zn-rich phases: pyroxene and spinel (Fig. 3).

The origin of coarse-grained segregations in pyrometallurgical slags

The coarse-grained segregations in the smelting slag from Katowice-Wełnowiec resemble miarolitic segregations found

Table 4 EPMA data (wt.%) for oxykinoshitalite-like mica and fluorapatite

	oks core	oks rim	fap	fap
Sb_2O_5	0.23	0.20	–	–
P_2O_5	–	–	39.66	40.57
SiO_2	35.52	39.15	1.23	1.09
	14.33	12.94	–	–
Y_2O_3	–	–	0.23	0.24
La_2O_3	–	–	0.32	0.36
Ce_2O_3	–	–	0.56	0.62
Pr_2O_3	–	–	0.19	0.00
Nd_2O_3	–	–	0.17	0.19
FeO	5.87	7.13	0.48	0.15
ZnO	0.42	0.72	–	–
MnO	0.16	0.37	–	–
MgO	22.3	22.19	–	–
CaO	–	–	54.5	54.16
BaO	7.64	2.60	–	–
Na_2O	0.73	1.16	–	–
K_2O	8.13	9.87	–	–
F	–	–	2.92	2.52
Total	95.31	96.31	100.26	99.9
a.p.f.u. (atoms per formula units)				
Sb^{5+}	0.01	0.01	–	–
P^{5+}	–	–	2.98	3.03
Si	2.96	3.14	0.11	0.1
Al	1.41	1.22	–	–
Y^{3+}	–	–	0.01	0.01
La^{3+}	–	–	0.01	0.01
Ce^{3+}	–	–	0.02	0.02
Pr^{3+}	–	–	0.01	0.00
Nd^{3+}	–	–	0.01	0.01
Fe^{2+}	0.41	0.48	0.04	0.01
Zn	0.03	0.04	–	–
Mn	0.01	0.02	–	–
Mg	2.77	2.65	–	–
Ca	–	–	5.18	5.12
Ba	0.25	0.08	–	–
Na	0.12	0.18	–	–
K	0.86	1.01	–	–
F	–	–	0.82	0.70
O^{2-}	12.00	12.00	13.00	13.00

oks–oxykinoshitalite, fap–fluorapatite

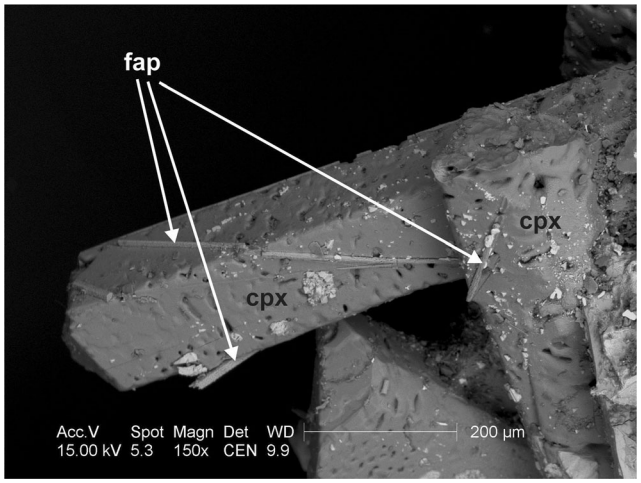

Fig. 9 Fluorapatite as inclusions pyroxene crystal. Abbreviations: cpx – clinopyroxene; fap – fluorapatite

in basalts and other volcanic rocks (e.g. Sparks 1978; Shea et al. 2010). By analogy to the origin of natural miarolitic cavities in igneous rocks, we suggest that residual liquid enriched in volatiles and Ca was originated during the fractional crystallization of molten slag. The residual volatile-rich liquid moved upwards until it encountered a solidified uppermost portion of the slag that cooled at the contact with air. That explains the ellipsoidal or irregular flattened shape of the segregations and their orientation parallel to the contact with the overlying vesicular slag (Fig. 1).

Perhaps CO_2 was the major volatile component of the molten slag due to the thermal dissociation of carbonates added as a fluxing material. The water activity was insignificant except for the border zone, in which hydrous mica crystallized. Fluorine and phosphorus activity was negligible and probably restricted to the latest stages of crystallization in miarolitic cavities leading to the crystallization of fluorapatite.

The high concentration of Zn in silicates and oxides in slags resulted from the non-efficient metal extraction in smelters (Warchulski et al. 2015; Warchulski 2015). All of major phases in the segregations (melilite, pyroxene, spinel) are enriched in Zn, relative to the bulk slag. Zinc concentrations in spinel series and pyroxenes in the segregations are an order of magnitude higher than in their counterparts in the surrounding slag (Fig. 11, Table 1). Intermediate concentrations of Zn occur in the border zone. The relative enrichment in Zn of segregations reflects the Zn preference for volatile phase as seen in magmatic systems (e.g. Nadeau et al. 2013 and references therein).

Considering both the reaction (1, 2) and the enrichment in Zn, the estimated temperature of crystallization of the segregations is above 1000 °C. This estimate is consistent with the temperature of the molten slag (1200–1300 °C) that was transported to the slag bed. The temperature of the overlain vesicular slag calculated from the olivine-bulk chemical composition is in the range of 1200–1350 °C, while calculations based on the clinopyroxene-bulk chemical composition give 1140–1260 °C (Warchulski 2015.).

Puziewicz et al. (2007) by analogy to rapidly cooled, but holocrystalline silica-undersaturated lavas assumed that low

Table 5 EPMA data (wt.%) for sulphides

	(Mn,Zn,Fe)S	(Mn,Zn,Fe)S	(Mn,Zn,Fe)S	(Mn,Zn,Fe)S	po	po	ccp	ccp	gn
Fe	14.98	14.6	27.97	28.21	58.76	58.54	38.00	38.41	0.29
Cu	0.17	0.48	0.12	-	-	0.25	23.56	23.3	0.04
Zn	46.21	46.5	21.26	21.08	-	0.15	1.22	1.49	-
S	33.59	33.46	49.34	49.27	38.83	39.48	35.07	34.42	13.06
Mn	4.12	4.53	0.99	0.91	0.16	0.05	0.67	0.76	0.13
As	0.14	0.09	-	-	0.01	-	0.04	-	0.11
Se	0.01	0.03	0.01	0.02	-	0.05	0.00	0.02	0.33
Pb	-	-	-	-	-	-	-	-	85.25
Ag	0.13	-	0.01	-	-	-	0.38	0.38	0.89
Sb	0.00	0.03	-	-	0.02	-	-	-	1.25
Co	0.02	-	-	0.06	0.13	0.01	0.12	0.11	0.14
Ni	-	-	-	-	0.14	0.07	0.13	-	-
Total	99.37	99.72	99.7	99.55	98.05	98.6	99.19	98.89	101.49
a.p.f.u. (atoms per formula units)									
Fe	0.26	0.25	0.56	0.57	0.87	0.85	0.62	0.64	0.01
Cu	0.00	0.01	0.00	-	-	0.00	0.34	0.34	0.00
Zn	0.67	0.68	0.43	0.42	-	0.00	0.02	0.02	-
S	1.00	1.00	1.00	1.00	1.00	1.00	1.00	1.00	0.99
Mn	0.07	0.08	0.02	0.02	0.00	0.00	0.01	0.01	0.01
As	0.00	0.00	-	-	0.00	-	0.00	-	0.00
Se	0.00	0.00	0.00	0.00	-	0.00	0.00	0.00	0.01
Pb	-	-	-	-	-	-	-	-	1.00
Ag	0.00	-	0.00	-	-	-	0.00	0.00	0.02
Sb	0.00	0.00	-	-	0.00	-	-	-	0.02
Co	0.00	-	-	0.00	0.00	0.00	0.00	-	-
Ni	-	-	-	-	0.00	0.00	0.00	0.00	0.00

(Mn,Zn,Fe)S-(Mn,Zn,Fe)S solid solution, po–pyrrhotite; ccp–chalcopyrite; gn–galena

viscosity is the key factor causing crystallization of slag-forming phases. In the border zone of the segregations the viscosity of the liquid increased due to the escape of volatiles into the cavities. That caused the increase in the nucleation rate in the border zone leading to the development of the fine-grained "aplitic" rim around the segregations (Figs. 2a-c). The accumulation of volatiles in the segregations caused the break-down of Si-O and Al-O bonds in the residual liquid. Some Al was also bound to Ca, Na, K and acted as melt modifier preventing the polymerization of Si-O-Si. That resulted in the decrease in viscosity of the melt and subsequently the decrease in the nucleation density resulting in the growth of the centimetre-sized euhedral or subhedral crystals (Fig. 3). Similarly to naturally occurring fractionation processes, the fractionated liquid became oxidized towards the centre of the segregation as suggested by the presence of trivalent Fe in leucite, spinels and hematite. The abundant sulphides in slag and border zones of the segregations reflect the enrichment in S caused by the thermal decomposition of ore sulphides under reducing conditions. They probably originated as a result of recrystallization of original sulphides, coupled with Fe-Mn incorporation into the new sulphide structure. The occurrence of sulphides in the slag suggests strong variability of the oxygen fugacity oscillating between MH and QMF buffers during melt crystallization.

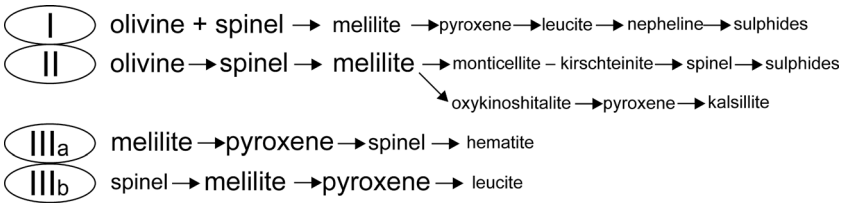

Fig. 10 The sequence of the crystallization in the crystalline slag (I), border zones (II), miarolitic segregations (IIIa), and in massive segregations (IIIb)

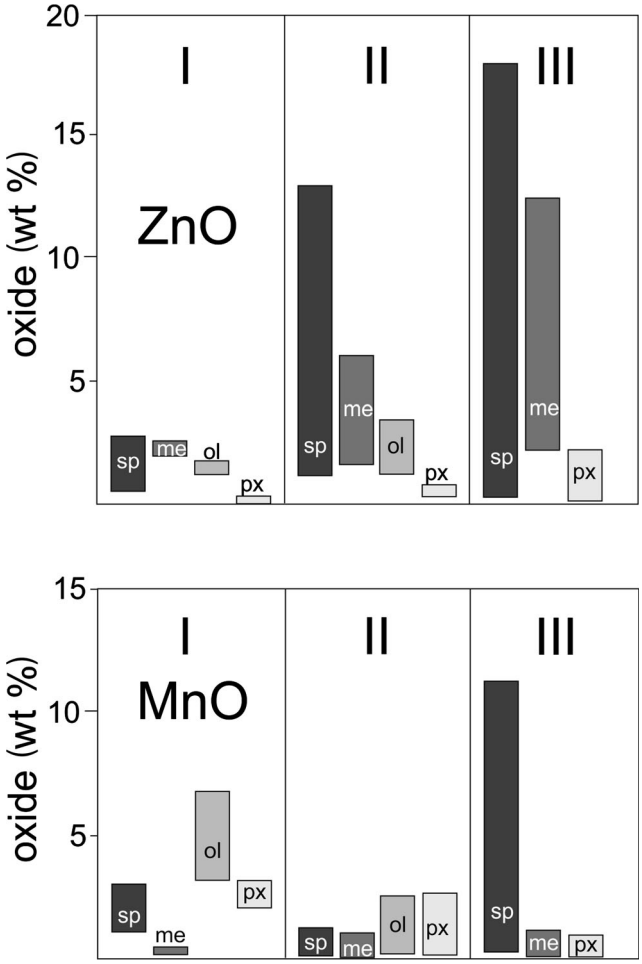

Fig. 11 Partitioning of Zn and Mn (as oxides) between mineral phases in slag (I), border zone (II) and segregations (III)

Phase compositions of the slag and the segregations are generally the same. However, the chemical compositions of the phases are significantly different (Fig. 11, Tables 1,and 3). Chemical zoning observed in major phases of pyrometallurgical slags (spinels, olivine, pyroxene) is indicative of the fractional crystallization (e.g. Ettler et al. 2001; Puziewicz et al. 2007; Kucha et al. 1996; Warchulski et al. 2015). The sector zoning in pyroxene crystals common in the miarolitic segregations is indicative of the disequilibrium growth, with different crystal faces attracting different cations as a result of different proportion of bonds at the crystal – melt interface (Dowty 1976) or can be an effect of different diffusion rates for the specific components in relation to crystal growth rate (Watson and Liang 1995). Both processes may have operated in slag and in segregations.

The deposition of the new portion of the hot slag (ca. 1250 °C) onto the surface of the investigated slag prevented the latter from rapid cooling and from volatiles to escape, enabling the formation of the holocrystalline slag with numerous coarse-grained segregations. The vesicular texture and the absence of the coarse-grained segregations in the overlying slag provide an evidence for its rapid degassing at the contact with air. The observed cross-section of two slags in Katowice-Wełnowiec resembles the layered intrusions formed by repeated magma batches maintaining the super-solidus conditions (e.g. Diaz-Alvarado et al. 2013) and, as in the case of the tabular intrusions – prevent volatiles from escaping forming the internal pegmatoidal structures (e.g. Gawęda et al. 2013).

Conclusions

The occurrence of coarse-grained segregations with euhedral crystals is a unique feature of the investigated slag from Katowice – Wełnowiec compared to other pyrometallurgical slags worldwide. The segregations originated from volatile-rich residual melt separated from molten slag during fractional crystallization. The formation of coarse-grained segregations was enabled by the fast deposition of vesicular slag on the top of the holocrystalline slag, acting as a thermal and physical barrier preventing the latter from rapid cooling and escape of volatiles.

Metallurgical silicate slags can be considered analogous to igneous rocks and as such they can provide additional insight into the behaviour of natural melts regardless their origin.

Acknowledgments We thank the reviewers for their constructive comments. This study was supported by National Science Center (NCN) through grant no. 2014/13/B/ST10/02403 to AG, and by the Polish Ministry of Science and Higher Education scholarship for young researchers: "Restoration of the historic smelting process at zinc smelter Katowice - Szopienice on the base of petrographic and geochemical data" to RW.

References

Álvarez-Valero AM, Sáez R, Pérez-López R, Delgado J, Nieto JM (2009) Evaluation of heavy metal bio-availability from almagrera pyrite-rich tailings dam (Iberian Pyrite Belt, SW Spain) based on a sequential extraction procedure. J Geochem Explor 102:87–94

Diaz-Alvarado J, Fernandez C, Castro A, Moreno-Ventas I (2013) SHRIMP U-Pb geochronology and thermal modelling of multilayer granitoid intrusions: implications for the building and thermal evolution of the Central System batholiths, Iberian massif, Spain. Lithos 175-176:104–123

Dowty E (1976) Crystal structure and crystal growth: II. sector zoning in minerals. Am Mineral 61:460–469

Ettler V, Johan Z (2014) 12 years of leaching of contaminants from Pb smelter slags: geochemical/mineralogical controls and slag recycling potential. Appl Geochem 40:97–103

Ettler V, Legendre O, Bodénan F, Touray J-C (2001) Primary phases and natural weathering of old lead-zinc pyrometalurgical slag from Příbram, Czech Republic. Can Mineral 39:873–888

Gawęda A, Müller A, Stein H, Kądziołko-Gaweł M, Mikulski S (2013) Age and origin of the tourmaline-rich hydraulic breccias in the tatra granite, Western Carpathians. J Geosci 58:133–158

Greiner P (2004) My land Katowice (moja ziemia Katowice). Publisher, Bractwo Gospodarcze Związku Górnośląskiego, Katowice, pp. 42–48

Gustafson WI (1974) The stability of andradite, hedenbergite and related minerals in the system Ca – Fe – Si – O – H. J Petrol 15:455–496

Heijlen W, Muchez P, Banks DA, Schneider J, Kucha H, Keppens E (2003) Carbonate-hosted Zn-Pb deposits in upper Silesia, Poland: origin and evolution of mineralizing fluids and constraints on genetic models. Econ Geol 98:911–932

Kierczak J, Bril H, Neel C, Puziewicz J (2010) Pyrometallurgical slags in upper and lower Silesia (Poland): from environmental risk to use of slag-based product – a review. Arch Environ Prot 36(3):111–126

Kogarko LN, Uvarova YA, Sokolova E, Hawthorne FC, Ottolini L, Grice JD (2005) Oxykinoshitalite, a new species of mica from Fernando de Noronha island, Pernambuco, Brazil: occurrence and crystal structure. Can Mineral 43:1501–1510

Kucha H, Martens A, Ottenburgs R, De Vos W, Viaene W (1996) Primary minerals of Zn-Pb mining and metallurgical dumps and their environmental behavior at Plombières, Belgium. Environ Geol 27:1–15

Kushiro I, Yoder HS (1964) Experimental studies on the basalt- eclogite transformation. Carnegie inst. Washington. Ann Rept Dir Geophys Lab 1964-65:89–94

Ladell J, Zagofsky A, Pearlman S (1975) Cu Kα2 elimination algorithm. J Appl Crystallogr 8:499–506

Mayer W, Sass-Gustkiewicz M (1998) Geochemical characterization of sulphide minerals from the olkusz lead-zinc ore cluster, upper Silesia, (Poland), based on laser ablation data. Mineral Pol 29:87–105

Nadeau O, Williams-Jones AE, Stix J (2013) Magmatic-hydrothermal evolution and devolatilization beneath merapi volcano, Indonesia. J Volcanol Geotherm Res 261:50–68

Piatak NM, Seal RR II (2010) Mineralogy and the release of trace elements from slag from the hegeler zinc smelter, Illinois (USA). Appl Geochem 25:302–320

Puziewicz J, Zainoun K, Bril H (2007) Primary phases in pyrometallurgical slags from a zinc-smelting waste dump, Świętochłowice, upper Silesia, Poland. Can Mineral 45:1189–1200

Rajchel B (2008) Geochemia Tl, As, Cd, Pb w rudach oraz odpadach hutniczych Zn-Pb Górnego Śląska. AGH University, Cracov, Doctoral thesis

Shea T, Houghton BF, Gurioli L, Cashman KV, Hammer JE, Hobden BJ (2010) Textural studies of vesicles in volcanic rocks: an integrated methodology. J Volcanol Geotherm Res 190:271–289

Sparks RSJ (1978) The dynamics of bubble formation and growth in magmas: a review and analysis. J Volcanol Geotherm Res 3:1–37

Sterns JG, Khasanov AM, Miller JW, Pollak H, Zhe L (1998) Mössbauer mineral handbook. Mössbauer Effect Data Center, Asheville, USA

Vernon RH (2004) A practical guide to Rock microstructure. Cambridge University Press

Vítková M, Ettler V, Johan Z, Kříbek B, Šebek O, Mihaljevič M (2010) Primary and secondary phases in copper-cobalt smelting slags from the Copperbelt Province, Zambia. Mineral Mag 74:581–600

Walter LS (1963) Experimental studies on Bowen's decarbonation series. I: P-T univariant equilibria of the 'monticellite' and 'akermanite' reactions. Am J Sci 261:488–500

Warchulski R (2015) Zn-Pb slag crystallization: evaluating temperature conditions on the basis of geothermometry. Eur J Mineral. doi:10.1127/ejm/2015/0027-2496

Warchulski R, Szopa K (2014) Phase composition of Katowice - Wełnowiec pyrometallurgical slags: preliminary SEM study. CTGeo 3:76–81

Warchulski R, Gawęda A, Kądziołka-Gaweł M, Szopa K (2015) Composition and element mobilization in pyrometallurgical slags from the Orzeł Biały smelting plant in the Bytom – piekary Śląskie area, Poland. Mineral Mag 79:459–483

Watson EB, Liang Y (1995) A simple model for sector zoning in slowly grown crystals: implications for growth rate and lattice diffusion, with emphasis on accessory minerals in crustal rocks. Am Mineral 80:1179–1187